PHOTONICS Research

Nonlinear optical properties of $CsPbCl_xBr_{3-x}$ nanocrystals embedded glass

Chenjing Quan,[1,2,†] Xiao Xing,[2,†] Sihao Huang,[2] Mengfeifei Jin,[3] Tongchao Shi,[2] Zeyu Zhang,[2,4,5] Weidong Xiang,[3,6] Zhanshan Wang,[1,7] and Yuxin Leng[2,4,8]

[1]School of Physics Science and Engineering, Tongji University, Shanghai 200092, China
[2]State Key Laboratory of High Field Laser Physics and CAS Center for Excellence in Ultra-intense Laser Science, Shanghai Institute of Optics and Fine Mechanics (SIOM), Chinese Academy of Sciences (CAS), Shanghai 201800, China
[3]College of Chemistry and Materials Engineering, Wenzhou University, Wenzhou 325035, China
[4]Hangzhou Institute for Advanced Study, University of Chinese Academy of Sciences, Hangzhou 310024, China
[5]School of Physics and Electronics, Shandong Normal University, Jinan 250014, China
[6]e-mail: xiangweidong001@126.com
[7]e-mail: wangzs@tongji.edu.cn
[8]e-mail: lengyuxin@mail.siom.ac.cn

Received 7 April 2021; revised 7 June 2021; accepted 22 June 2021; posted 22 June 2021 (Doc. ID 427155); published 23 August 2021

All-inorganic perovskite has attracted significant attention due to its excellent nonlinear optical characteristics. Stable and low-toxic perovskite materials have great application prospects in optoelectronic devices. Here, we study the nonlinear optical properties of $CsPbCl_xBr_{3-x}$ ($x = 1, 1.5, 2$) nanocrystals (NCs) glass by open-aperture Z-scan. It is found that the two- (2PA) and three-photon absorption (3PA) intensity can be adjusted by the treatment temperature and the ratio of halide anions. The perovskite NCs glass treated at a high temperature has better crystallinity, resulting in stronger nonlinear absorption performance. In addition, the value of the 2PA parameter of $CsPbCl_{1.5}Br_{1.5}$ NCs glasses decreases when the incident pump intensity increases, which is ascribed to the saturation of 2PA and population inversion. Finally, the research results show that the 2PA coefficient ($0.127\ \mathrm{cm\,GW^{-1}}$) and 3PA coefficient ($1.21 \times 10^{-5}\ \mathrm{cm^3\,GW^{-2}}$) of $CsPbCl_1Br_2$ NCs glass with high Br anion content are larger than those of $CsPbCl_2Br_1$ and $CsPbCl_{1.5}Br_{1.5}$ NCs glasses. This is mainly due to the greater influence of Br anions on the symmetry of the perovskite structure, which leads to the redistribution of delocalized electrons. The revealed adjustable nonlinear optical properties of perovskite NCs glass are essential for developing stable and high-performance nonlinear optical devices.

https://doi.org/10.1364/PRJ.427155

1. INTRODUCTION

All-inorganic perovskite has received widespread attention recently, owing to its tunable light-emitting bandgap [1,2], large exciton binding energy [3], and other excellent photoelectric properties [4,5]. Hence, perovskite materials are mostly used in light-emitting diodes (LEDs) [6,7], solar cells [8], photodetectors [9,10], lasers [4,11], and other devices. Halide perovskite nanocrystals have become one of the most promising optoelectronic materials due to their low-cost and easy synthesis [1]. Compared with bulk and layered materials, the specific surface area of $CsPbCl_xBr_{3-x}$ nanocrystals (NCs) is greatly increased, thereby enhancing the NC optical performance [1,2,12]. Due to the strong multiphoton absorption (MPA) characteristics of halide perovskite NCs, they are very promising as a material for the development of multiphoton pump lasers [13]. The spherical NCs not only overcome the difficulty of large area growth of thin films, but also can combine with a variety of substrates or solutions for incorporation into optoelectronic devices [14].

Owing to the poor stability of bare perovskite and toxicity of lead halide perovskite, the application of perovskite materials in optoelectronic devices is greatly restricted [15,16]. So far, diverse approaches to improve the stability of perovskite materials have been reported, such as bonding of the organic ligands [17], establishing core/shell nanostructure [18], Mn-doping [19], silica coating [20,21], and infiltrating $CsPbX_3$ NCs into mesoporous matrices [22]. However, combining the thermal, chemical, and mechanical stability of the glass has been proved an effective method to improve the stability of perovskite NCs [23–25]. Hu *et al*. reported the well-designed arrangement of $CsPbBr_3$ NCs glasses with reduced self-absorption emission and enhanced the quantum efficiency of solar cells [26]. Ye *et al*. investigated the versatile precipitation of $CsPbX_3$ NCs glasses, in which photoluminescence (PL) covering the whole visible range with high efficiency could be achieved [24].

Meanwhile, some researches indicated that the relative PL intensity of $CsPbBr_3$ quantum dots glass is still ~85% ~ 90% after being immersed in water for 120 h or exposed to UV light for 100 h, and even about 60% of PL intensity still remained for storage up to 45 days [27,28]. All these previous studies reveal that embedding $CsPbX_3$ quantum dots or NCs into glass has a great potential in improving its stability and fluorescence performance [26–28].

However, the nonlinear optical aspect of perovskite glass, especially the study of MPA, which is important to the application of these optoelectronic devices, has been rarely investigated [13,29,30]. Many studies have been reported on the nonlinear optical properties of pure perovskite [31]. For example, a two-photon absorption (2PA) cross section of $CsPbBr_3$ NCs in toluene as high as 10^6 GW has been reported [32]. Chen *et al.* demonstrated that the 2PA cross section of $CsPbBr_3$ NCs depends on the particle size [33]. Furthermore, due to the symmetry breaking of the perovskite octahedron structure, Li *et al.* confirmed that all-inorganic perovskites with different proportions of halogen atoms show greater MPA intensity than $CsPbCl_3$ and specially designed organic molecules [34,35]. Not only that, Chen *et al.* reported that the five-photon absorption cross section of Type-I core-shell halide perovskite NCs is 9 orders of magnitude higher than that of specially designed organic molecules [30]. However, the nonlinear optical aspect of perovskite glass, which is highly desired for applications in low-threshold lasing [36], optical data storage [37], photodetectors [38], and other nonlinear optical photoelectric devices [32], has been rarely investigated.

In the present work, the three-order nonlinear optical characteristics of $CsPbCl_xBr_{3-x}$ ($x = 1$, 1.5, 2) NCs glasses have been investigated by open-aperture (OA) Z-scan measurements using femtosecond laser pulses. We observe the 2PA and three-photon absorption (3PA) phenomena of $CsPbCl_xBr_{3-x}$ ($x = 1$, 1.5, 2) NCs glasses at wavelengths of 800 and 1300 nm. The magnitude of the 2PA coefficient (β) of $CsPbCl_xBr_{3-x}$ ($x = 1$, 1.5, 2) NCs glasses is about 10^{-1}–10^{-2} $\mathrm{cm\,GW^{-1}}$, and the magnitude of the 3PA coefficient (γ) is 10^{-5}–10^{-6} $\mathrm{cm^3\,GW^{-2}}$. The observed MPA behavior of $CsPbCl_xBr_{3-x}$ ($x = 1$, 1.5, 2) NCs glasses could play a great role in the development of perovskite-based optoelectronic devices.

2. EXPERIMENT SETUP

In the OA Z-scan measurement, as shown as Fig. 1, the perovskite NCs glasses with thickness L are moved along the Gaussian light propagation direction, and the laser beam transmittance after the sample is measured. For 2PA measurement, we used a Ti:sapphire femtosecond laser (Spectra-Physics) operating at a central wavelength of 800 nm with a repetition frequency of 1 kHz and a pulse width of 35 fs. For 3PA measurements, the laser source consisted of an optical parametric amplifier (TOPAS-Prime), delivering a wavelength of 1300 nm with a pulse width of 200 fs. The repetition frequency of laser was 1 kHz. In order to amplify weak signals, a chopper (Thorlabs MC2000B) is inserted into the optical path. The focal length of the front lens of the sample is 10 cm, and the spot radius at the focal point is about 30 μm. The transmitted intensity of each pulse after passing through the sample is measured by a Si-biased detector (Thorlabs DET10A2) using the lock-in amplifier (Signal Recovery Model 7270) technique.

3. RESULTS AND DISCUSSION

In this work, $CsPbCl_xBr_{3-x}$ ($x = 1$, 1.5, 2) NCs are successfully embedded inside a glass sheet (radius = 10 mm, thickness = 0.56 mm) matrix via the melt-quenching and *in situ* crystallization method. The $CsPbCl_xBr_{3-x}$ ($x = 1$, 1.5, 2) NCs are spherical structures with a diameter of ~35–45 nm [see the Appendix A, Fig. 6(a)] [39]. Figure 2(a) shows the X-ray diffraction (XRD) patterns of $CsPbCl_{1.5}Br_{1.5}$ NCs glass under different treatment temperatures. The diffraction peaks of perovskite glass are at 15.5°, 22°, 31°, 38.5°, and 44.6°, corresponding to (100), (110), (200), (211), and (220) phase, respectively [40,41]. Referring to the previous research results, these narrow diffraction peaks demonstrate that the $CsPbCl_{1.5}Br_{1.5}$ NCs have good crystallization [25]. Figure 2(b) displays the PL emission spectra of $CsPbCl_{1.5}Br_{1.5}$ NCs glass. The PL emission peak of

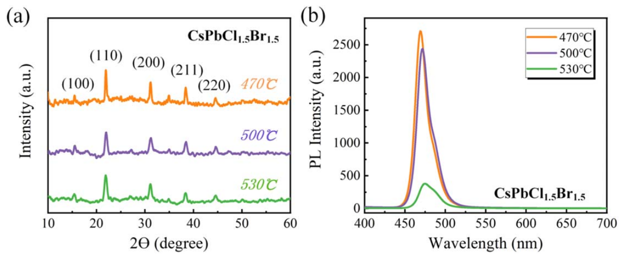

Fig. 2. (a) XRD patterns and (b) PL emission spectra of $CsPbCl_{1.5}Br_{1.5}$ NCs glasses under different treatment temperature excited by femtosecond pulses at 365 nm.

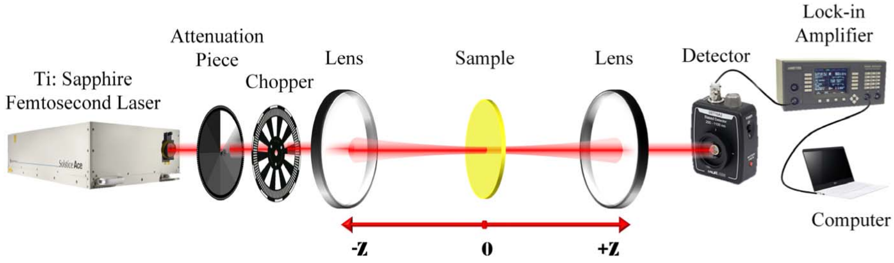

Fig. 1. Experimental setup for the Z-scan technique.

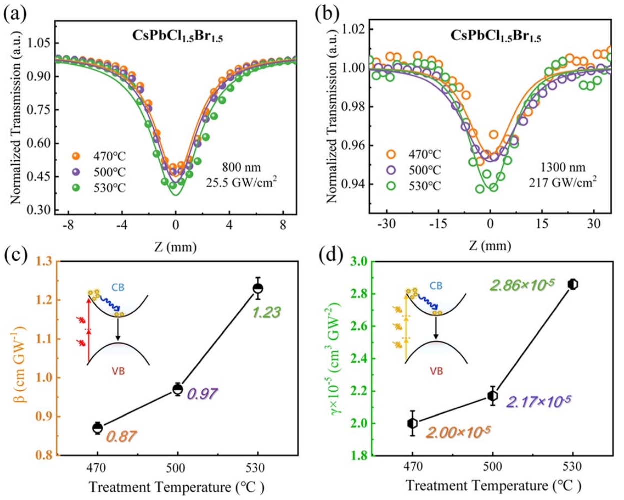

Fig. 3. OA Z-scan results of $CsPbCl_{1.5}Br_{1.5}$ NCs glasses with different treatment temperatures. (a) Under pump intensity 25.5 GW/cm^2 at a wavelength of 800 nm and (b) under pump intensity 217 GW/cm^2 at a wavelength of 1300 nm. (The balls are the experimental data, and the solid lines are fitting curves.) The fitting results of (c) β and (d) γ of $CsPbCl_{1.5}Br_{1.5}$ NCs glass with different treatment temperatures. (Inset, the schematic of a two-level model.)

$CsPbCl_{1.5}Br_{1.5}$ NCs glass displays a slight redshift with the treatment temperature from 470°C to 530°C. The reason for the slight redshift of PL emission peak in the $CsPbCl_{1.5}Br_{1.5}$ NCs glass is the increase of the crystal grains size, which is caused by the increase of the heat treatment temperature [41]. However, the surface defects increase due to the continuous increase in temperature, which affects the fluorescence quantum yield and causes the PL emission intensity of the $CsPbCl_{1.5}Br_{1.5}$ NCs glass to decrease [41].

Figures 3(a) and 3(b) show the OA Z-scan curves of the $CsPbCl_{1.5}Br_{1.5}$ NCs glass (bandgap ~ 2.58 eV) at the different treatment temperature excited by 800 nm (~1.55 eV) with pump intensity of 25.5 GW/cm^2 and by 1300 nm (~0.95 eV) with pump intensity of 217 GW/cm^2, respectively (see the Appendix A, Fig. 8). As shown in Figs. 3(a) and 3(b), the Z-scan curves are all valley shapes. When the $CsPbCl_{1.5}Br_{1.5}$ NCs glass is close to the focus, the normalized transmission of the incident laser decreases. As shown in Figs. 3(a) and 3(b), the $CsPbCl_{1.5}Br_{1.5}$ NCs glass with a heat treatment temperature of 530°C has the strongest nonlinear response.

In theory, the measured normalized transmission (T) for OA Z-scan results is given by the expression [42,43]

$$T_{OA(nPA)} = \frac{1}{\{1 + (n-1)\alpha_{NL}L_{eff}\{I_0/[1+(z/z_0)^2]\}^{n-1}\}^{1/n-1}} \quad (n = 1, 2, 3), \tag{1}$$

where L_{eff} is the effective length of the sample. α_{NL} is the nonlinear optical coefficient. z is the position of the sample in the light path, $z_0 = \pi\omega_0^2/\lambda$ is the Rayleigh range of the Gaussian beam, and ω_0 is the beam waist at the focal point ($z = 0$).

Among them, the 2PA coefficient is represented by β. The imaginary part of third-order nonlinear susceptibility [44,45],

$$\mathrm{Im}\chi^{(3)} = \frac{c^2\varepsilon_0 n_0^2\beta}{\omega}, \tag{2}$$

where c is the speed of light, n_0 is the linear refractive index, and ε_0 and ω are the vacuum permittivity and angular frequency of the laser beam, respectively. The figures of merit (FOMs) are used to describe nonlinear absorption characteristics: FOM $= |\mathrm{Im}\chi^{(3)}/\alpha_0|$, where α_0 is the linear absorption coefficient. The 3PA coefficient is represented by γ. The effective thicknesses of 2PA and 3PA are $L_{eff} = (1 - e^{-\alpha_0 L})/\alpha_0$ and $L'_{eff} = (1 - e^{-2\alpha_0 L})/2\alpha_0$, respectively [42,43].

Figures 3(c) and 3(d) display the 2PA and 3PA coefficients of $CsPbCl_{1.5}Br_{1.5}$ NCs glasses at the different treatment temperatures obtained by fitting Eq. (1). The insets in Figs. 3(c) and 3(d) show the schematic diagram of the 2PA and 3PA processes, respectively. When $CsPbCl_{1.5}Br_{1.5}$ NCs glass is excited by the femtosecond laser, electrons in the valence band need to absorb two (or three) photons at the same time to transition to the conduction band. By fitting with a Z-scan theory, 2PA coefficients of $CsPbCl_{1.5}Br_{1.5}$ NCs glass with different treatment temperatures were calculated: $\beta = 0.87$ cm GW^{-1} for 470°C treatment temperature, $\beta = 0.97$ cm GW^{-1} for 500°C treatment temperature, and $\beta = 1.23$ cm GW^{-1} for 530°C treatment temperature, respectively. Under the pump intensity of 25 GW/cm^2, the $\mathrm{Im}\chi^{(3)}$ for $CsPbCl_{1.5}Br_{1.5}$ NCs glasses are in the range of (1.99–2.81) × 10^3 esu and the magnitudes of FOM are all at 10^3 esu cm obtained by fitting Eq. (2) (see the Appendix A, Table 1). 3PA coefficients of $CsPbCl_{1.5}Br_{1.5}$ NCs glasses with different treatment temperatures were calculated: $\gamma = 2 \times 10^{-5}$ cm^3 GW^{-2} for 470°C, $\gamma = 2.17 \times 10^{-5}$ cm^3 GW^{-2} for 500°C, and $\gamma = 2.86 \times 10^{-5}$ cm^3 GW^{-2} for 530°C, respectively. As the processing temperature increases, the crystallinity is better. The larger the nanocrystal particles, the stronger the 2PA and 3PA performance of the $CsPbCl_{1.5}Br_{1.5}$ NCs glasses [39].

Furthermore, the nonlinear properties of $CsPbCl_{1.5}Br_{1.5}$ NCs glasses with different pump intensities are measured. The OA Z-scan curves of $CsPbCl_{1.5}Br_{1.5}$ NCs glass under 500°C treatment temperature with various incident pump intensities at the wavelength of 800 nm are shown in Fig. 4(a). The normalized transmittance decreases when either increasing the pump intensity or placing the $CsPbCl_{1.5}Br_{1.5}$ NCs glass closer to the focus point, $z = 0$, while as the pump intensity

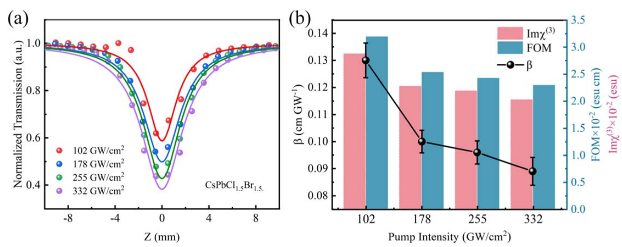

Fig. 4. (a) OA Z-scan curves and (b) corresponding fitting results of β (black ball), $\mathrm{Im}\chi^{(3)}$ (pink), and FOM (blue) of the $CsPbCl_{1.5}Br_{1.5}$ NCs glass at the wavelength of 800 nm with different incident pump intensity.

increases, the normalized transmittance curve deepens. These results suggest the potential application of $CsPbCl_{1.5}Br_{1.5}$ NCs glass in optoelectronic devices, such as optical limiting devices [46]. Figure 4(b) summarizes the dependence of 2PA fitting results as a function of pump intensity. (Fitting results are summarized in Table 2). The β is 0.096 cm/GW of $CsPbCl_{1.5}Br_{1.5}$ NCs glass at the pump intensity of 255 GW/cm^2 and 0.089 cm/GW at the pump intensity of 332 GW/cm^2, respectively. The result of the 2PA coefficient we obtained is with the same order of magnitude as the $CsPbBr_3$ NCs [36] and $CsPbCl_xBr_{3-x}$ ($x = 1$, 2) quantum dots [47]. The perovskite NCs encapsulated in perovskite glass are isolated from the external environment. This gives them better stability and greatly improves the service life of perovskite NCs. The $\mathrm{Im}\chi^{(3)}$ for $CsPbCl_{1.5}Br_{1.5}$ NCs glasses are in the range of $(2.03–2.88) \times 10^2$ esu and the FOM is in the range of $(2.3–3.2) \times 10^2$ esu cm. It is shown that as the pump intensity increased, the value of β, $\mathrm{Im}\chi^{(3)}$, and FOM decreased. The same phenomenon has been observed in other materials, such as PbS/glue nanocomposite [48] and few-layer WS_2 films [49]. As the incident light energy increases, a large number of carriers gather in the excited state, resulting in population inversion [50]. Hence, the electrons in the ground state cannot further absorb the photon and transition to the excited state [51]. The β of $CsPbCl_{1.5}Br_{1.5}$ NCs decreases as the pump intensity increases.

To further explore the influence of different doped halogen anion ratios on the MPA and consider the influence of treatment temperature on the PL performance of all-inorganic perovskite glasses, we choose $CsPbCl_xBr_{3-x}$ ($x = 1$, 1.5, 2) NCs glasses with a treatment temperature of 500°C to explore their nonlinear response [52]. Figures 5(a) and 5(b) display the OA Z-scan response of $CsPbCl_xBr_{3-x}$ ($x = 1$, 1.5, 2) NCs glasses under femtosecond laser of 800 nm and 1300 nm, respectively.

Figure 5(a) shows the OA Z-scan curves of $CsPbCl_xBr_{3-x}$ ($x = 1$, 1.5, 2) NCs glasses under pump intensity 178 GW/cm^2 at a wavelength of 800 nm. Comparing the normalized transmittance curves of $CsPbCl_xBr_{3-x}$ ($x = 1$, 1.5, 2) NCs glasses with different Cl^- and Br^- ion ratios, it is found that the $CsPbCl_xBr_{3-x}$ ($x = 1$, 1.5, 2) NCs glasses with higher Br^- ions doping ratio have a greater nonlinear response in the process of 2PA and 3PA. The bandgap width of $CsPbCl_1Br_2$ NCs glasses is 2.46 eV, slightly smaller than that of $CsPbCl_{1.5}Br_{1.5}$ (2.58 eV) and $CsPbCl_2Br_1$ (2.7 eV) (see the Appendix A, Fig. 8). Due to the increase of Br^- ion content, the bandgap is narrowed, thereby promoting the carrier transition rate [34,53]. $CsPbCl_1Br_2$ NCs glasses exhibit a large MPA phenomenon. Correspondingly, the PL emission peak of $CsPbCl_2Br_1$, $CsPbCl_{1.5}Br_{1.5}$, and $CsPbCl_1Br_2$ NCs glasses with emission wavelength peaks at 454, 470, and 490 nm is shown in Fig. 5(c), respectively. The PL peak shifts to the lower energy direction as the proportion of Br^- ions increases. It is shown that the luminescence can be effectively tuned by introducing the Cl^- and Br^- ion ratios. The width of $CsPbCl_xBr_{3-x}$ ($x = 1$, 1.5, 2) NCs glasses at half-height (FWHM) of the PL emission is less than 30 nm (see the Appendix A, Fig. 7).

By fitting the Z-scan data in Figs. 5(a) and 5(b), the β of $CsPbCl_1Br_2$ NCs glass is ~0.087 $cm\,GW^{-1}$, 0.1 $cm\,GW^{-1}$ for $CsPbCl_{1.5}Br_{1.5}$ NCs glass, and 0.127 $cm\,GW^{-1}$ for $CsPbCl_2Br_1$ NCs glass. The 2PA coefficient of $CsPbCl_1Br_2$ NCs glass is 1 order of magnitude higher than that of $CsPbCl_1Br_2$ quantum dots [47]. Combined with Eq. (2), the $\mathrm{Im}\chi^{(3)}$ for $CsPbCl_xBr_{3-x}$ NCs glasses is in a range of $(1.99–2.9) \times 10^2$ esu, which is larger than that of $CsPbBr_3$ NC (see the Appendix A). The FOM value used to describe the nonlinear absorption characteristics is in the range of $(2.2–2.53) \times 10^2$ esu cm (see the Appendix A, Table 3). Meanwhile, we obtained the γ: 0.54×10^{-5} $cm^3\,GW^{-2}$ is for $CsPbCl_2Br_1$ NCs glass, 0.82×10^{-5} $cm^3\,GW^{-2}$ is for $CsPbCl_{1.5}Br_{1.5}$ NCs glass, and 1.21×10^{-5} $cm^3\,GW^{-2}$ is for $CsPbCl_1Br_2$ NCs glass. The 3PA coefficient of $CsPbCl_1Br_2$ NCs glass is over 1 order of magnitude larger than that of the $CsPbCl_{1.5}Br_{1.5}$ and $CsPbCl_2Br_1$ NCs glasses. This is mainly because the $CsPbCl_1Br_2$ NCs glass has a narrower bandgap and higher structural destabilization that will lead to the easier carrier transition and delocalized electrons redistribution compared with $CsPbCl_{1.5}Br_{1.5}$ and $CsPbCl_2Br_1$ NCs

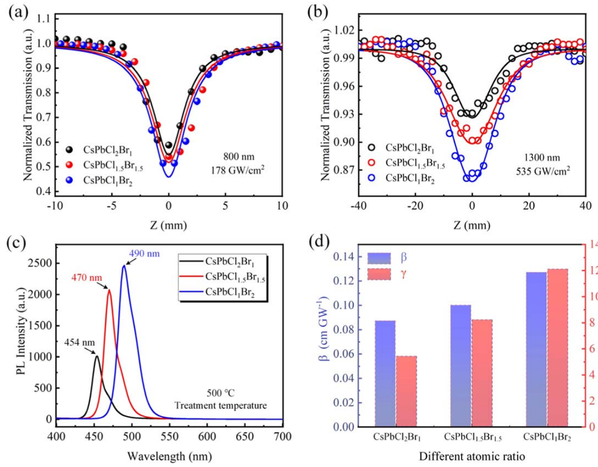

Fig. 5. OA Z-scan results of $CsPbCl_xBr_{3-x}$ ($x = 1$, 1.5, 2) NCs glasses. (a) Under pump intensity 178 GW/cm^2 at a wavelength of 800 nm and (b) under pump intensity 535 GW/cm^2 at a wavelength of 1300 nm. (The balls are the experimental data, and the solid lines are fitting curves.) (c) PL emission spectra of $CsPbCl_xBr_{3-x}$ ($x = 1$, 1.5, 2) NCs glasses for 500°C treatment temperature excited by femtosecond pulses at 365 nm; (d) fitting the results of 2PA coefficient (β, purple bar) and 3PA coefficient (γ, red bar) obtained in (a) and (b), respectively.

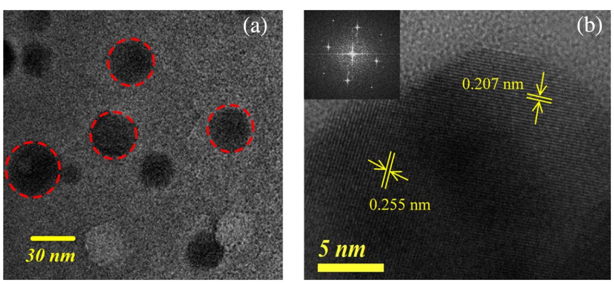

Fig. 6. (a) Transmission electron microscopy (TEM) images of $CsPbCl_xBr_{3-x}$ ($x = 1$, 1.5, 2) NCs and (b) high-resolution TEM images of $CsPbCl_{1.5}Br_{1.5}$ NCs.

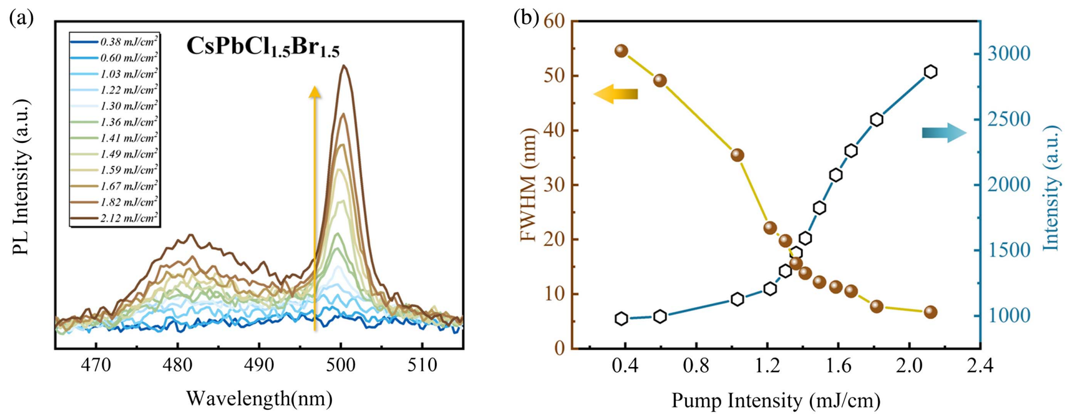

Fig. 7. (a) Amplified spontaneous emission (ASE) measurement on $CsPbCl_{1.5}Br_{1.5}$ NCs glass under an 800 nm pulsed laser at room temperature and (b) corresponding full-width at half-maxima (FWHM) and output as a function of incident pump intensity.

glasses [24]. Due to the narrower bandgap and structural destabilization of the perovskite, the electron cloud is distorted, which promotes the transition of electrons from the ground state to the excited state [34]. Therefore, the carrier transition rate is further increased.

4. CONCLUSION

In summary, we measure the 2PA and 3PA properties of $CsPbCl_xBr_{3-x}$ ($x = 1, 1.5, 2$) NCs glasses using the OA Z-scan method. The $CsPbCl_{1.5}Br_{1.5}$ NCs glass under 530°C treatment temperature exhibited the strongest 2PA and 3PA coefficients, which is mainly due to the better crystallization properties of perovskite NCs at higher temperatures. Furthermore, the dependence of incident pump intensity shows that the nonlinear coefficient decreases when the incident pump intensity increases. We also found that the larger the proportion of Br anions, the stronger the MPA performance. These results for $CsPbCl_xBr_{3-x}$ NCs glass may guide designs for their potential use in applications.

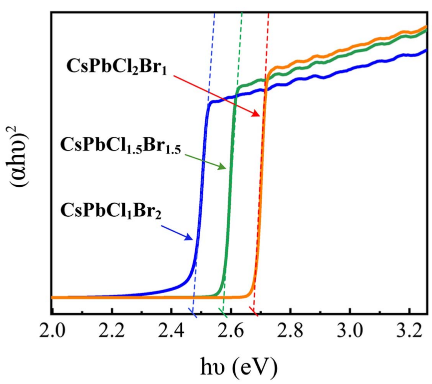

Fig. 8. $(\alpha h\upsilon)^2$-$h\upsilon$ plot of $CsPbCl_xBr_{3-x}$ ($x = 1, 2, 3$) NCs glass.

APPENDIX A

The $CsPbCl_xBr_{3-x}$ ($x = 1, 1.5, 2$) nanocrystals are spherical structures with a diameter of ~35–45 nm enclosed in a glass sheet, as shown in Fig. 6(a). As shown as Fig. 9, $CsPbCl_1Br_2$ and $CsPbCl_2Br_1$ NCs glasses also showed the 2PA phenomenon that the normalized transmittance decreased greatly as the pump power increased under the wavelength of 800 nm. As the pump energy becomes stronger, more carriers are excited,

Table 2. 2PA Parameters of the $CsPbCl_{1.5}Br_{1.5}$ NCs Glass Measured by an OA Z-Scan at 800 nm under Different Pump Intensity[a]

Pump Intensity (GW/cm^2)	β (cm GW^{-1})	$\mathrm{Im}\chi^{(3)}$ (esu)	FOM (esu cm)
102	0.13 ± 0.0064	2.88×10^2	3.2×10^2
178	0.1 ± 0.0042	2.28×10^2	2.54×10^2
255	0.096 ± 0.0043	2.19×10^2	2.43×10^2
332	0.089 ± 0.0052	2.03×10^2	2.3×10^2

[a] β, 2PA coefficient; $\mathrm{Im}\chi^{(3)}$, imaginary part of third-order nonlinear susceptibility; FOM, figures of merit.

Table 1. Summary of the Measured 2PA and 3PA Parameters of $CsPbCl_{1.5}Br_{1.5}$ NCs Glasses at Wavelengths of 800 nm and 1300 nm[a]

Sample	Growth Condition	T	α_0 (cm^{-1})	β (cm GW^{-1})	γ ($\times 10^{-5}$ cm^3 GW^{-2})	$\mathrm{Im}\chi^{(3)}$ (esu)	FOM (esu cm)
$CsPbCl_{1.5}Br_{1.5}$	470°C	0.94	0.48	0.87 ± 0.015	2 ± 0.077	1.99×10^3	4.14×10^3
$CsPbCl_{1.5}Br_{1.5}$	500°C	0.90	0.81	0.97 ± 0.016	2.17 ± 0.058	2.21×10^3	2.73×10^3
$CsPbCl_{1.5}Br_{1.5}$	530°C	0.88	0.99	1.23 ± 0.028	2.86 ± 0.031	2.81×10^3	2.84×10^3

[a] T, linear transmittance of perovskite glasses; α_0, linear absorption coefficient; β, 2PA coefficient; γ, 3PA coefficient; $\mathrm{Im}\chi^{(3)}$, imaginary part of third-order nonlinear susceptibility; FOM, figures of merit.

Table 3. Summary of the Measured 2PA and 3PA Parameters of $CsPbCl_xBr_{3-x}$ NCs Glasses at Wavelengths of 800 nm and 1300 nm[a]

Sample	Growth Condition	T	α_0 (cm^{-1})	β ($\times10^{-2}$ cm GW^{-1})	γ ($\times10^{-5}$ cm^3 GW^{-2})	Im$\chi^{(3)}$ (esu)	FOM (esu cm)
$CsPbCl_2Br_1$	500°C	0.89	0.9	8.7 ± 0.42	0.54 ± 0.017	1.99×10^2	2.2×10^2
$CsPbCl_{1.5}Br_{1.5}$	500°C	0.89	0.9	10 ± 0.59	0.82 ± 0.02	2.28×10^2	2.53×10^2
$CsPbCl_1Br_2$	500°C	0.85	1.26	12.7 ± 0.52	1.21 ± 0.02	2.9×10^2	2.3×10^2

[a] T, linear transmittance of perovskite glasses; α_0, linear absorption coefficient; β, 2PA coefficient; γ, 3PA coefficient; Im$\chi^{(3)}$, imaginary part of third-order nonlinear susceptibility; FOM, figures of merit.

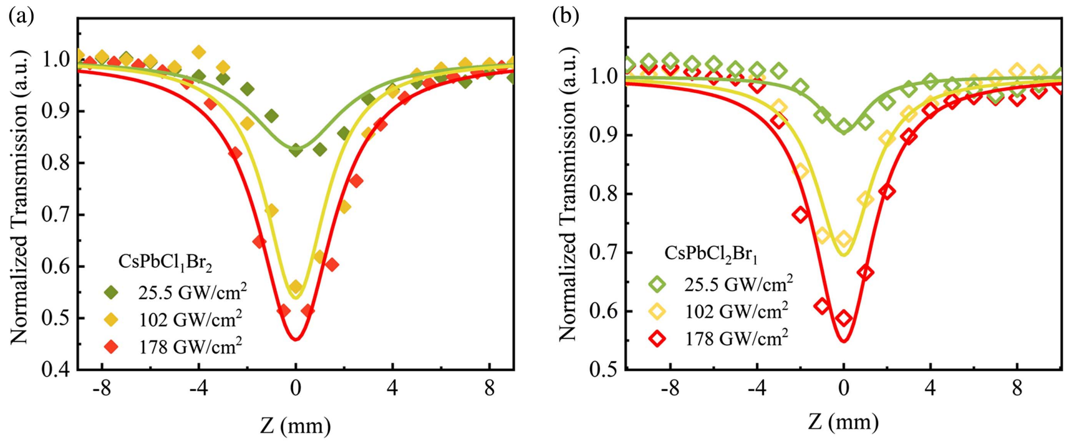

Fig. 9. Open-aperture Z-scan curves of the (a) $CsPbCl_1Br_2$ and (b) $CsPbCl_2Br_1$ NCs glasses at the wavelength of 800 nm with different incident pump intensity.

thereby absorbing more photons. This performance can be applied to optoelectronic devices such as optical limiting.

Funding. National Natural Science Foundation of China (61520106012, 61674023, 61875211, 61905264, 61925507); National Key Research and Development Program of China (2017YFE0123700); Strategic Priority Research Program of the Chinese Academy of Sciences (XDB16030400); CAS Interdisciplinary Innovation Team; Program of Shanghai Academic/Technology Research Leader (18XD1404200); Shanghai Municipal Science and Technology Major Project (2017SHZDZX02).

Disclosures. The authors declare no conflicts of interest.

†These authors contributed equally to this work.

REFERENCES

1. L. Protesescu, S. Yakunin, M. I. Bodnarchuk, F. Krieg, R. Caputo, C. H. Hendon, R. X. Yang, A. Walsh, and M. V. Kovalenko, "Nanocrystals of cesium lead halide perovskites ($CsPbX_3$, X = Cl, Br, and I): novel optoelectronic materials showing bright emission with wide color Gamut," Nano Lett. **15**, 3692–3696 (2015).
2. G. Nedelcu, L. Protesescu, S. Yakunin, M. I. Bodnarchuk, M. J. Grotevent, and M. V. Kovalenko, "Fast anion-exchange in highly luminescent nanocrystals of cesium lead halide perovskites ($CsPbX_3$, X = Cl, Br, I)," Nano Lett. **15**, 5635–5640 (2015).
3. J. A. Castaneda, G. Nagamine, E. Yassitepe, L. G. Bonato, O. Voznyy, S. Hoogland, A. F. Nogueira, E. H. Sargent, C. H. Cruz, and L. A. Padilha, "Efficient biexciton interaction in perovskite quantum dots under weak and strong confinement," ACS Nano **10**, 8603–8609 (2016).
4. S. Chen and G. Shi, "Two-dimensional materials for halide perovskite-based optoelectronic devices," Adv. Mater. **29**, 1605448 (2017).
5. T. Zhang, M. I. Dar, G. Li, F. Xu, N. Guo, M. Grätzel, and Y. Zhao, "Bication lead iodide 2D perovskite component to stabilize inorganic α-$CsPbI_3$ perovskite phase for high-efficiency solar cells," Sci. Adv. **3**, e1700841 (2017).
6. H. Cho, S.-H. Jeong, M.-H. Park, Y.-H. Kim, C. Wolf, C.-L. Lee, J. H. Heo, A. Sadhanala, N. Myoung, S. Yoo, S. H. Im, R. H. Friend, and T.-W. Lee, "Overcoming the electroluminescence efficiency limitations of perovskite light-emitting diodes," Science **350**, 1222–1225 (2015).
7. Z. K. Tan, R. S. Moghaddam, M. L. Lai, P. Docampo, R. Higler, F. Deschler, M. Price, A. Sadhanala, L. M. Pazos, D. Credgington, F. Hanusch, T. Bein, H. J. Snaith, and R. H. Friend, "Bright light-emitting diodes based on organometal halide perovskite," Nat. Nanotechnol. **9**, 687–692 (2014).
8. J. Yang, X. Wen, H. Xia, R. Sheng, Q. Ma, J. Kim, P. Tapping, T. Harada, T. W. Kee, F. Huang, Y. B. Cheng, M. Green, A. Ho-Baillie, S. Huang, S. Shrestha, R. Patterson, and G. Conibeer, "Acoustic-optical phonon up-conversion and hot-phonon bottleneck in lead-halide perovskites," Nat. Commun. **8**, 14120 (2017).
9. M. Li, S. Bhaumik, T. W. Goh, M. S. Kumar, N. Yantara, M. Gratzel, S. Mhaisalkar, N. Mathews, and T. C. Sum, "Slow cooling and highly efficient extraction of hot carriers in colloidal perovskite nanocrystals," Nat. Commun. **8**, 14350 (2017).
10. X. Qi, Y. Zhang, Q. Ou, S. T. Ha, C. W. Qiu, H. Zhang, Y. B. Cheng, Q. Xiong, and Q. Bao, "Photonics and optoelectronics of 2D metal-halide perovskites," Small **14**, 1800682 (2018).
11. J. Butkus, P. Vashishtha, K. Chen, J. K. Gallaher, S. K. K. Prasad, D. Z. Metin, G. Laufersky, N. Gaston, J. E. Halpert, and J. M. Hodgkiss, "The evolution of quantum confinement in $CsPbBr_3$ perovskite nanocrystals," Chem. Mater. **29**, 3644–3652 (2017).

12. J. He, L. Tao, H. Zhang, B. Zhou, and J. Li, "Emerging 2D materials beyond graphene for ultrashort pulse generation in fiber lasers," Nanoscale **11**, 2577–2593 (2019).
13. A. Pramanik, K. Gates, Y. Gao, S. Begum, and P. C. Ray, "Several orders-of-magnitude enhancement of multiphoton absorption property for $CsPbX_3$ perovskite quantum dots by manipulating halide stoichiometry," J. Phys. Chem. C **123**, 5150–5156 (2019).
14. H. C. Wang, Z. Bao, H. Y. Tsai, A. C. Tang, and R. S. Liu, "Perovskite quantum dots and their application in light-emitting diodes," Small **14**, 1702433 (2018).
15. G. E. Eperon, S. N. Habisreutinger, T. Leijtens, B. J. Bruijnaers, J. J. Franeker, D. W. deQuilettes, S. Pathak, R. J. Sutton, G. Grancini, D. S. Ginger, R. A. J. Janssen, A. Petrozza, and H. J. Snaith, "The importance of moisture in hybrid lead halide perovskite thin film fabrication," ACS Nano **9**, 9380–9393 (2015).
16. C. Sun, Y. Zhang, C. Ruan, C. Yin, X. Wang, Y. Wang, and W. W. Yu, "Efficient and stable white LEDs with silica-coated inorganic perovskite quantum dots," Adv. Mater. **28**, 10088–10094 (2016).
17. F. Palazon, Q. A. Akkerman, M. Prato, and L. Manna, "X-ray lithography on perovskite nanocrystals films: from patterning with anion-exchange reactions to enhanced stability in air and water," ACS Nano **10**, 1224–1230 (2016).
18. V. K. Ravi, S. Saikia, S. Yadav, V. V. Nawale, and A. Nag, "$CsPbBr_3$/ZnS core/shell type nanocrystals for enhancing luminescence lifetime and water stability," ACS Energy Lett. **5**, 1794–1796 (2020).
19. W. J. Mir, A. Swarnkar, and A. Nag, "Postsynthesis Mn-doping in $CsPbI_3$ nanocrystals to stabilize the black perovskite phase," Nanoscale **11**, 4278–4286 (2019).
20. F. Zhang, Z. Shi, S. Li, Z. Ma, Y. Li, L. Wang, D. Wu, Y. Tian, G. Du, X. Li, and C. Shan, "Synergetic effect of the surfactant and silica coating on the enhanced emission and stability of perovskite quantum dots for anticounterfeiting," ACS Appl. Mater. Interfaces **11**, 28013–28022 (2019).
21. F. Zhang, Z. F. Shi, Z. Z. Ma, Y. Li, S. Li, D. Wu, T. T. Xu, X. J. Li, C. X. Shan, and G. T. Du, "Silica coating enhances the stability of inorganic perovskite nanocrystals for efficient and stable down-conversion in white light-emitting devices," Nanoscale **10**, 20131–20139 (2018).
22. D. N. Dirin, L. Protesescu, D. Trummer, I. V. Kochetygov, S. Yakunin, F. Krumeich, N. P. Stadie, and M. V. Kovalenko, "Harnessing defect-tolerance at the nanoscale: highly luminescent lead halide perovskite nanocrystals in mesoporous silica matrixes," Nano Lett. **16**, 5866–5874 (2016).
23. M. Xia, J. Luo, C. Chen, H. Liu, and J. Tang, "Semiconductor quantum dots-embedded inorganic glasses: fabrication, luminescent properties, and potential applications," Adv. Opt. Mater. **7**, 1900851 (2019).
24. Y. Ye, W. Zhang, Z. Zhao, J. Wang, C. Liu, Z. Deng, X. Zhao, and J. Han, "Highly luminescent cesium lead halide perovskite nanocrystals stabilized in glasses for light-emitting applications," Adv. Opt. Mater. **7**, 1801663 (2019).
25. B. Ai, C. Liu, J. Wang, J. Xie, J. Han, X. Zhao, and J. Heo, "Precipitation and optical properties of $CsPbBr_3$ quantum dots in phosphate glasses," J. Am. Ceram. Soc. **99**, 2875–2877 (2016).
26. Y. Hu, W. Zhang, Y. Ye, Z. Zhao, and C. Liu, "Femtosecond-laser-induced precipitation of $CsPbBr_3$ perovskite nanocrystals in glasses for solar spectral conversion," ACS Appl. Nano Mater. **3**, 850–857 (2019).
27. S. Yuan, D. Chen, X. Li, J. Zhong, and X. Xu, "*In situ* crystallization synthesis of $CsPbBr_3$ perovskite quantum dot-embedded glasses with improved stability for solid-state lighting and random upconverted lasing," ACS Appl. Mater. Interfaces **10**, 18918–18926 (2018).
28. X. Pang, H. Zhang, L. Xie, T. Xuan, Y. Sun, S. Si, B. Jiang, W. Chen, J. Zhuang, C. Hu, Y. Liu, B. Lei, and X. Zhang, "Precipitating $CsPbBr_3$ quantum dots in boro-germanate glass with a dense structure and inert environment toward highly stable and efficient narrow-band green emitters for wide-color-gamut liquid crystal displays," J. Mater. Chem. C **7**, 13139–13148 (2019).
29. J. Li, Q. Jing, S. Xiao, Y. Gao, Y. Wang, W. Zhang, X. W. Sun, K. Wang, and T. He, "Spectral dynamics and multiphoton absorption properties of all-inorganic perovskite nanorods," J. Phys. Chem. Lett. **11**, 4817–4825 (2020).
30. W. Chen, S. Bhaumik, S. A. Veldhuis, G. Xing, Q. Xu, M. Gratzel, S. Mhaisalkar, N. Mathews, and T. C. Sum, "Giant five-photon absorption from multidimensional core-shell halide perovskite colloidal nanocrystals," Nat. Commun. **8**, 15198 (2017).
31. G. Nagamine, J. O. Rocha, L. G. Bonato, A. F. Nogueira, Z. Zaharieva, A. A. R. Watt, C. H. de Brito Cruz, and L. A. Padilha, "Two-photon absorption and two-photon-induced gain in perovskite quantum dots," J. Phys. Chem. Lett. **9**, 3478–3484 (2018).
32. Y. Xu, Q. Chen, C. Zhang, R. Wang, H. Wu, X. Zhang, G. Xing, W. W. Yu, X. Wang, Y. Zhang, and M. Xiao, "Two-photon-pumped perovskite semiconductor nanocrystal lasers," J. Am. Chem. Soc. **138**, 3761–3768 (2016).
33. J. Chen, P. Chabera, T. Pascher, M. E. Messing, R. Schaller, S. Canton, K. Zheng, and T. Pullerits, "Enhanced size selection in two-photon excitation for $CsPbBr_3$ perovskite nanocrystals," J. Phys. Chem. Lett. **8**, 5119–5124 (2017).
34. J. Z. Li, C. Ren, X. Qiu, X. D. Lin, R. Chen, C. Yin, and T. C. He, "Ultrafast optical nonlinearity of blue-emitting perovskite nanocrystals," Photon. Res. **6**, 554–559 (2018).
35. J. Li, F. Zhao, S. Xiao, J. Cheng, X. Qiu, X. Lin, R. Chen, and T. He, "Giant two- to five-photon absorption in $CsPbBr_{2.7}I_{0.3}$ two-dimensional nanoplatelets," Opt. Lett. **44**, 3873–3876 (2019).
36. Y. Wang, X. Li, X. Zhao, L. Xiao, H. Zeng, and H. Sun, "Nonlinear absorption and low-threshold multiphoton pumped stimulated emission from all-inorganic perovskite nanocrystals," Nano Lett. **16**, 448–453 (2016).
37. B. Nafradi, P. Szirmai, M. Spina, H. Lee, O. V. Yazyev, A. Arakcheeva, D. Chernyshov, M. Gibert, L. Forro, and E. Horvath, "Optically switched magnetism in photovoltaic perovskite $CH_3NH_3(Mn:Pb)I_3$," Nat. Commun. **7**, 13406 (2016).
38. G. Tong, H. Li, Z. Zhu, Y. Zhang, L. Yu, J. Xu, and Y. Jiang, "Enhancing hybrid perovskite detectability in the deep ultraviolet region with down-conversion dual-phase ($CsPbBr_3$-Cs_4PbBr_6) films," J. Phys. Chem. Lett. **9**, 1592–1599 (2018).
39. M. Jin, S. Huang, C. Quan, X. Liang, J. Du, Z. Liu, Z. Zhang, and W. Xiang, "Blue low-threshold room-temperature stimulated emission from thermostable perovskite nanocrystals glasses through controlling crystallization," J. Eur. Ceram. Soc **41**, 1579–1585 (2021).
40. L. Y. Bai, S. W. Wang, Y. W. Zhang, K. X. Zhang, and L. X. Yi, "Influence of annealing process on the stable luminous $CsPbCl_3$ perovskite films by thermal evaporation," J. Lumin. **227**, 117592 (2020).
41. E. Erol, O. Kıbrıslı, M. Ç. Ersundu, and A. E. Ersundu, "Size-controlled emission of long-time durable $CsPbBr_3$ perovskite quantum dots embedded tellurite glass nanocomposites," Chem. Eng. J. **401**, 126053 (2020).
42. K. N. Krishnakanth, S. Seth, A. Samanta, and S. V. Rao, "Broadband ultrafast nonlinear optical studies revealing exciting multi-photon absorption coefficients in phase pure zero-dimensional Cs_4PbBr_6 perovskite films," Nanoscale **11**, 945–954 (2019).
43. L. Wu, Y. Dong, J. Zhao, D. Ma, W. Huang, Y. Zhang, Y. Wang, X. Jiang, Y. Xiang, J. Li, Y. Feng, J. Xu, and H. Zhang, "Kerr nonlinearity in 2D graphdiyne for passive photonic diodes," Adv. Mater. **31**, 1807981 (2019).
44. C. Quan, M. He, C. He, Y. Huang, L. Zhu, Z. Yao, X. Xu, C. Lu, and X. Xu, "Transition from saturable absorption to reverse saturable absorption in $MoTe_2$ nano-films with thickness and pump intensity," Appl. Surf. Sci. **457**, 115–120 (2018).
45. X. Jiang, L. Zhang, S. Liu, Y. Zhang, Z. He, W. Li, F. Zhang, Y. Shi, W. Lü, Y. Li, Q. Wen, J. Li, J. Feng, S. Ruan, Y.-J. Zeng, X. Zhu, Y. Lu, and H. Zhang, "Ultrathin metal-organic framework: an emerging broadband nonlinear optical material for ultrafast photonics," Adv. Opt. Mater. **6**, 1800561 (2018).
46. D. Andres-Penares, J. Navarro-Arenas, R. I. Sánchez-Alarcón, R. Abargues, J. P. Martínez-Pastor, and J. F. Sánchez-Royo, "Enhanced optical response of InSe nanosheet devices decorated with $CsPbX_3$ (X=I, Br) perovskite nanocrystals," Appl. Surf. Sci. **536**, 147939 (2021).
47. Q. Han, W. Wu, W. Liu, Q. Yang, and Y. Yang, "Two-photon absorption and upconversion luminescence of colloidal $CsPbX_3$ quantum dots," Opt. Mater. **75**, 880–886 (2018).

48. P. A. Kurian, C. Vijayan, C. S. Suchand Sandeep, R. Philip, and K. Sathiyamoorthy, "Two-photon-assisted excited state absorption in nanocomposite films of PbS stabilized in a synthetic glue matrix," Nanotechnology **18**, 075708 (2007).
49. N. D. S. Zhang, N. McEvoy, M. O'Brien, S. Winters, N. C. Berner, C. Yim, Y. Li, X. Zhang, Z. Chen, G. S. Duesberg, and J. Wang, "Direct observation of degenerate two-photon absorption and its saturation in WS_2 and MoS_2 monolayer and few-layer films," ACS Nano **9**, 7142–7150 (2015).
50. J. Wang, B. Gu, X.-W. Ni, and H.-T. Wang, "Z-scan theory with simultaneous two- and three-photon absorption saturation," Opt. Laser Technol. **44**, 390–393 (2012).
51. B. Gu, Y.-X. Fan, J. Chen, H.-T. Wang, J. He, and W. Ji, "Z-scan theory of two-photon absorption saturation and experimental evidence," J. Appl. Phys. **102**, 083101 (2007).
52. J. Chen, K. Zidek, P. Chabera, D. Liu, P. Cheng, L. Nuuttila, M. J. Al-Marri, H. Lehtivuori, M. E. Messing, K. Han, K. Zheng, and T. Pullerits, "Size- and wavelength-dependent two-photon absorption cross-section of $CsPbBr_3$ perovskite quantum dots," J. Phys. Chem. Lett. **8**, 2316–2321 (2017).
53. T.-H. Le, S. Lee, E. Heo, U. Lee, H. Lee, H. Jo, K. S. Yang, M. Chang, and H. Yoon, "Controlled anisotropic growth of layered perovskite nanocrystals for enhanced optoelectronic properties," Chem. Eng. J. **416**, 128045 (2021).